

This item is the archived peer-reviewed author-version of:

Three-dimensional nanoparticle transformations captured by an electron microscope

Reference:

Albrecht Wiebke, Van Aert Sandra, Bals Sara.- Three-dimensional nanoparticle transformations captured by an electron microscope
Accounts of chemical research - ISSN 0001-4842 - 54:5(2021), p. 1189-1199
Full text (Publisher's DOI): <https://doi.org/10.1021/ACS.ACCOUNTS.0C00711>
To cite this reference: <https://hdl.handle.net/10067/1776440151162165141>

3D Nanoparticle Transformations Captured by an Electron Microscope

Wiebke Albrecht, Sandra Van Aert, Sara Bals**

EMAT and NANOLab Center of Excellence, University of Antwerp, B-2020 Antwerp,
Belgium

CONSPECTUS

The three-dimensional (3D) morphology and composition govern the properties of nanoparticles (NPs). However, due to their high surface-to-volume ratio, the morphology and composition of nanomaterials are not as static as for their bulk counterparts. One major influence is the increase in relative contribution of surface diffusion, which underlines rapid reshaping of NPs in response to changes in their environment. If not accounted for, these effects might affect the robustness of prospective NPs in practically relevant conditions, such as elevated temperatures, intense light illumination or changing chemical environments. *In situ* techniques are promising tools to study NP transformations under relevant conditions. Among those tools, *in situ* transmission electron microscopy (TEM) provides an elegant platform to directly visualize NP changes down to the atomic scale. By using specialized holders or microscopes, external stimuli such as heat, or environments such as gas and liquids, can be controllably introduced inside the TEM. In addition, TEM is also a valuable tool to determine NP transformations upon *ex situ* stimuli such as laser excitation. However, standard TEM yields 2D projection images of 3D objects. With the growing complexity of NPs' shapes and compositions, the information that is obtained in this manner is often insufficient to understand intricate diffusion dynamics.

In this Account, we describe recent progress on measuring NP transformations in 3D inside the electron microscope. First, we discuss existing possibilities to obtain 3D information using either tomographic methods or the so-called atom counting technique, which utilizes single projection images. Next, we show how these techniques can be combined with *in situ* holders to quantify diffusion processes on a single nanoparticle level. Specifically, we focus on anisotropic metal NPs at elevated temperatures and varying gas environments. Anisotropic metal NPs are important for plasmonic applications, because sharp tips and edges result in strong electromagnetic field enhancements. By electron tomography, surface diffusion as well as elemental diffusion can be tracked in monometallic and bimetallic NPs, which can then be directly related to changes in plasmonic properties of these systems. By atom counting, it has furthermore become possible to monitor the evolution of crystalline facets of metal NPs under gas and heat treatments, a change that influences catalytic properties. Next to *in situ* processes, we also demonstrate the value of electron tomography to assess external laser-induced NP transformations, making it viable to detect structural changes with atomic resolution. The application of the proposed methodologies is by far not limited to metal nanoparticles. In the final section we therefore outline future material research that can benefit from tracking NP transformations from 3D techniques.

KEY REFERENCES

- Altantzis, T.; Lobato, I.; De Backer, A.; Béch e, A.; Zhang, Y.; Basak, S.; Porcu, M.; Xu, Q.; S anchez-Iglesias, A.; Liz-Marz an, L. M.; Van Tendeloo, G.; Van Aert, S.; Bals, S. Three-Dimensional Quantification of the Facet Evolution of Pt Nanoparticles in a Variable Gaseous Environment. *Nano Lett.* **2019**, 19, 477-481.¹ *A quantitative methodology was implemented to measure variations of the 3D atomic structure of catalytic Pt nanoparticles under the flow of selected gases; revealing that the particles*

exhibited a facet morphology with {100} and {111} planes under H₂ environment and a rounded morphology with a decreased percentage of those planes in O₂.

- Albrecht, W.; Bladt, E.; Vanrompay, H.; Smith, J. D.; Skrabalak, S. E.; Bals, S. Thermal Stability of Gold/Palladium Octopods Studied *in Situ* in 3D: Understanding Design Rules for Thermally Stable Metal Nanoparticles. *ACS Nano* **2019**, 13, 6522-6530.² *In situ electron tomography revealed that the addition of a low amount of Pd significantly enhances the thermal stability of nanoparticles and that next to particle composition, morphology and chemical environment are key parameters for designing thermally stable multifunctional nanoparticles.*
- Skorikov, A.; Albrecht, W.; Bladt, E.; Xie, X.; van der Hoeven, J. E. S.; van Blaaderen, A.; Van Aert, S.; Bals, S. Quantitative 3D Characterization of Elemental Diffusion Dynamics in Individual Ag@Au Nanoparticles with Different Shapes. *ACS Nano* **2019**, 13, 13421-13429.³ *Quantitative HAADF-STEM tomography was employed to measure in situ the 3D elemental diffusion dynamics in individual Au-Ag nanoparticles upon heating; allowing to determine diffusion coefficients on a single particle level as a function of shape, size and composition.*
- Milagres de Oliveira, T.; Albrecht, W.; González-Rubio, G.; Altantzis, T.; Lobato Hoyos, I. P.; Béché, A.; Van Aert, S.; Guerrero-Martínez, A.; Liz-Marzán, L. M.; Bals, S. 3D Characterization and Plasmon Mapping of Gold Nanorods Welded by Femtosecond Laser Irradiation. *ACS Nano* **2020**, 14, 12558-12570.⁴ *Atomic resolution tomography revealed that femtosecond laser welding of gold nanorods results in a single crystal defect at the welding interface, causing a significant plasmon broadening compared to single-crystalline nanorods, which could be unambiguously measured by electron energy loss spectroscopy.*

1. INTRODUCTION

Nanomaterials are of crucial importance in a broad range of applications including nanomedicine, catalysis, sensing, data storage or plasmonics. It is known that the functional properties of these materials are determined by their 3D structure and composition. Furthermore, organic ligands on the surface of the nanocrystals play an important role in the stabilization and chemical properties of the inorganic nanomaterials.⁵ If one is able to measure the positions of the atoms, their chemical nature and the bonding between them, it becomes possible to predict the physicochemical properties of the nanomaterials and one may therefore guide the development of novel nanostructures. For this purpose, quantitative 3D characterization techniques that yield information even down to the atomic scale are clearly indispensable.

Aberration corrected transmission electron microscopes (TEM) allow one to characterize materials with a spatial resolution of the order of 50 pm.⁶⁻⁹ Next to structural information, chemical and electronic knowledge can be obtained as well. However, TEM images are only two-dimensional (2D) projections of three-dimensional (3D) (nano)-objects. The development of electron tomography has created a powerful tool to explore the morphology, 3D structure and composition of a broad range of materials.¹⁰⁻¹³ Although these experiments are already at the state-of-the-art, several open questions remain. These questions are often related to the fact that 3D characterization by TEM is typically performed using the conventional conditions of a TEM: ultra-high vacuum and room temperature. Since it is known that the morphology and consequently, the activity of nanomaterials will transform at higher temperatures or pressures, this poses a fundamental limitation. It is therefore not surprising that a lot of effort has been devoted to monitor NP transformations upon external stimuli by TEM.¹⁴ For irreversible transformations, NPs can be exposed to such stimuli outside the microscope and investigated afterwards, allowing even for a direct comparison of the same NP before and after the stimuli.^{15,16} This approach is particularly indispensable for measuring NP transformations under stimuli, which are challenging to introduce inside the TEM, for instance laser excitation.

For reversible processes and to obtain dynamic information, *in situ* TEM characterization is valuable. Essentially two different technologies exist to perform these measurements. A so-called “Environmental TEM” (ETEM) is a dedicated TEM in which a differential pumping system separates the increased pressure in the sample area from the high vacuum regions surrounding the sample. Another possibility is the use of *in situ* holders. Currently, a wide variety of holders is available, ranging from the application of strain, heat and light to electric biasing. Furthermore, different environments such as liquids and gasses can now be created in a TEM using environmental cells. All of these exciting opportunities have transformed the TEM from a post mortem technique into a true nanolab, enabling the investigation of transformations of nanomaterials, *in situ* and at the highest possible resolution. However, understanding the complex changes for anisotropic nanosystems in 3D rather than in 2D remains very challenging. In this Account, we discuss recently developed tools that enabled us to investigate morphological and chemical changes of nanomaterials at high temperature, in a gaseous environment and upon laser irradiation. In the final section, we will provide an outlook for insights that can be gained from the described methodologies and describe future challenges in the field of 3D imaging of dynamic processes and NP transformations.

2. 3D INFORMATION IN THE ELECTRON MICROSCOPE

For a conventional electron tomography experiment, the sample holder is tilted in the TEM over a large tilt angle range to create a tilt series of projection images. Hereby, the tilt increment is typically 1° or 2° (**Figure 1a,b**). After alignment of this tilt series of projection images by e.g. cross correlation, it is combined into a 3D reconstruction through a mathematical algorithm (**Figure 1c**). An optimal reconstruction of the original object is retrieved with a full tilt range of 180° and fine tilt sampling. Unfortunately, this is not easily achievable in TEMs due to the limited space in-between the pole pieces of the objective lens. This lack of information due to the limited angular range is referred to as missing wedge.^{12,13} Nonetheless, accurate

reconstructions of the 3D object can be obtained with well-designed tomography holders, which allow for a typical tilt range of $\pm 75^\circ$, in combination with modern reconstruction algorithms.¹⁷

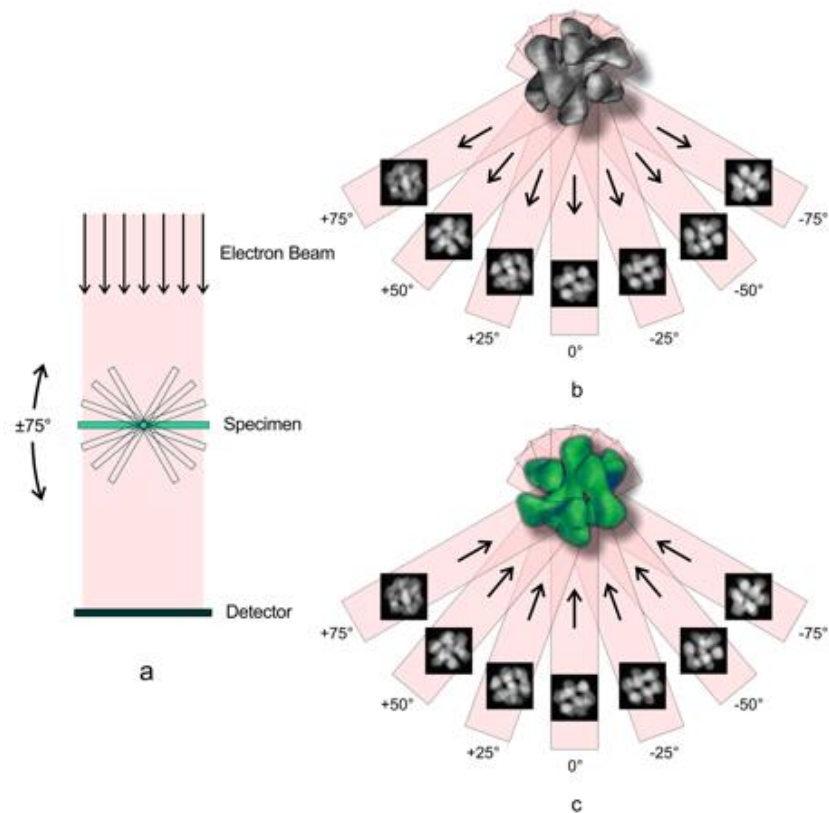


Figure 1. Illustration of a conventional electron tomography experiment, including the acquisition of a tilt series (a,b) and back-projection of the images along their original acquisition directions to obtain the object's 3D shape (c). The actual tilt range is limited due to the confined space in-between the pole pieces of the objective lens and due to shadowing of holders and TEM support grids. Thin tomography holders allow for a relatively large tilting range of $\pm 75^\circ$, whereas bulky *in situ* holders, such as gas or liquid holders, are generally more limited in tilt range (around $\pm 30^\circ$).

Over the years, different electron microscopy techniques such as Bright-Field (BF) TEM, high-angle annular dark-field scanning TEM (HAADF-STEM), electron holography, energy dispersive X-ray spectroscopy (EDX) and energy filtered TEM (EFTEM) have all been extended to 3D, providing a variety of novel insight on structure-function relationships for a

broad range of samples.^{12,13,18-20} Atomic resolution electron tomography has been the ultimate dream for many years. Although it is not yet possible to perform such experiments on all types of samples, significant progress has been achieved over the last decade.²¹⁻²⁶ In this manner, 3D strain measurements became possible and also disordered structures could be unraveled.^{27,28,29,30} However, all of these experiments resulted in static 3D snapshots of the nanostructures under investigation. Consequently, these results carry little information concerning the behavior of the nanomaterials during applications. Being able to visualize 3D transformations of the nanomaterials would therefore be an ideal tool to optimize the functionalities of nanostructures for a broad range of applications, such as catalysis, sensing and plasmonics.

Although recently developed *in situ* holders allow to apply a large variety of external stimuli, performing 3D characterization using these holders is very challenging. There are technical limitations, such as the narrow tilt range of some holders, but also more fundamental aspects such as the time required to collect the tilt series of images. Indeed, even a trained user needs at least 1 hour to acquire a high quality HAADF-STEM tilt series for conventional electron tomography. First attempts to accelerate the acquisition process of an electron tomography tilt series were already made a few years ago.³¹ Experiments at high temperature have also been performed using a dedicated ETEM and BF-TEM tomography.³² Unfortunately, several artefacts may arise, e.g. related to the relatively small tilt range over which the images were acquired.

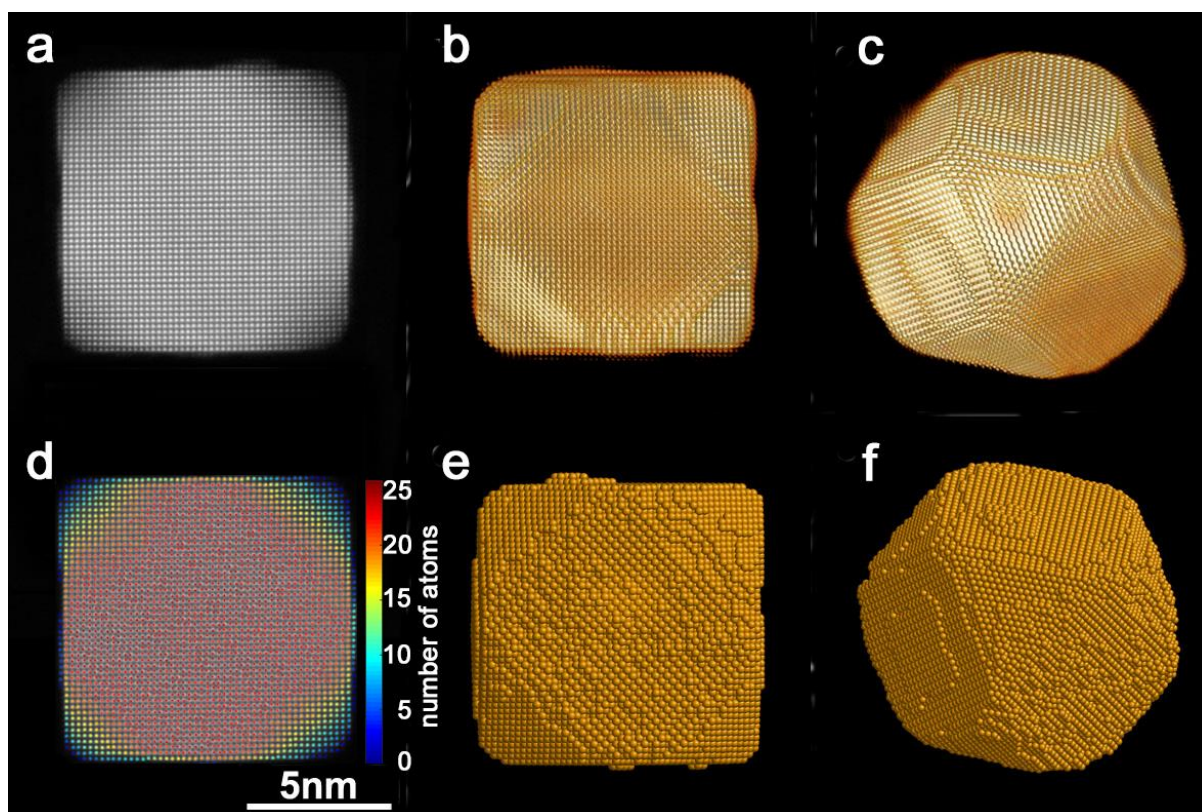


Figure 2. Comparison of the reconstructions based on atomic resolution tomography and those obtained by atom counting with energy minimization for a Pt nanoparticle. (a) High-resolution HAADF-STEM image which was used for conventional high-resolution electron tomography and for atom counting. (b,c) Three-dimensional visualization of the reconstructed nanoparticle obtained by conventional high-resolution tomography along different viewing directions. (d) Atom counts. (e,f) Three-dimensional models obtained using atom counting with energy minimization. Adapted with permission from ref. 1. Copyright 2019 American Chemical Society.

Moreover, when investigating highly scattering nano-objects, which is often the case for inorganic nanomaterials, diffraction contrast present in BF-TEM violates the projection requirement for tomography leading to artefacts in the reconstruction.¹² We therefore recently developed fast HAADF-STEM tomography,³³ which allowed us to decrease the acquisition time of a HAADF-STEM tomography series to a few minutes. The technique and its comparison to other fast electron tomography procedures is discussed in more detail

elsewhere.³⁴ By combining the approach with a Micro-Electro-Mechanical Systems (MEMS) heating holder able to tilt over a range of $\pm 80^\circ$, the technique has been proven to be of great interest to measure transformations of morphology and composition as a function of temperature. Examples of these investigations will be presented in Section 3.

Unfortunately, fast tomography is not always applicable, e.g. the tilt range of most gas cell holders does not allow one to obtain high quality 3D visualisations using conventional reconstruction algorithms. Alternatively, it is possible to estimate 3D models from single 2D HAADF-STEM projection images with the help of atom counting.^{22,35} By making use of an empirical model-based approach, so-called scattering cross sections are obtained at the atomic level.³⁶ Then, the distribution of the scattering cross-sections of all atomic columns is decomposed into overlapping normal distributions, which allows counting the number of atoms in a particular atomic column with single-atom sensitivity.³⁵ This approach was already used to investigate the dynamical behavior of ultra-small Ge clusters.³⁷ To extend the 2D images into 3D for these small clusters, *ab initio* calculations were performed, using different starting configurations, in agreement with the experimental 2D HAADF-STEM images. Also for larger nanoparticles, counting results can be applied to build a 3D model when combined with molecular dynamics (MD) simulations. This is illustrated for a Pt nanoparticle in **Figure 2**.¹ The high-resolution image shown in **Figure 2a** was part of a tomography series and could also be employed for atom counting. The 3D visualizations of the resulting reconstructions using the conventional simultaneous iterative reconstruction technique (SIRT) are shown in **Figures 2b,c**. The atom counting results, corresponding to **Figure 2a**, are shown in **Figure 2d** and were used to create a 3D starting configuration by positioning the atoms in each atomic column symmetrically around a central plane. Next, by using MD simulations employing the embedded atom method potential, a relaxed 3D structural model was obtained (**Figures 2e,f**). The comparison between the 3D reconstructions based on atomic resolution tomography and those obtained by atom counting with energy minimization shows very good agreement. Therefore,

we recently expanded this methodology to estimate transformations of the 3D structure of nanomaterials when exposed to high temperatures or a gaseous environment. In this manner, we obtained unique insights in the structure-property connection under realistic conditions, which will be discussed in Section 4.

3. TRANSFORMATIONS CAPTURED BY ELECTRON TOMOGRAPHY

As outlined in Section 2, it has recently become possible to monitor heat-induced transformations in 3D by using heating tomography holders. In this manner, we were able to not only quantify surface diffusion processes but also elemental diffusion inside single nanoparticles, which will be discussed in the first part of this section. These experiments were carried out in a stop-and-go manner, where heating cycles were interrupted to acquire tomography tilt series and were focussed on anisotropic metal NPs.

Anisotropic NPs, such as Au nanostars (NSs), are promising for a range of applications, including surface-enhanced Raman scattering, biomedical applications, or for generating hot electrons. These applications depend on the anisotropic shape of the NPs and their sharp tips. However, anisotropic metal NPs are known to reshape at temperatures hundreds of degrees below their bulk melting temperature.³⁸ In a first application of our recently developed fast HAADF-STEM tomography, we studied the transformation of highly anisotropic Au NSs at 200°C, 300°C and 400°C *in situ* using a DENSolutions heating tomography holder (**Figure 3a**).³³

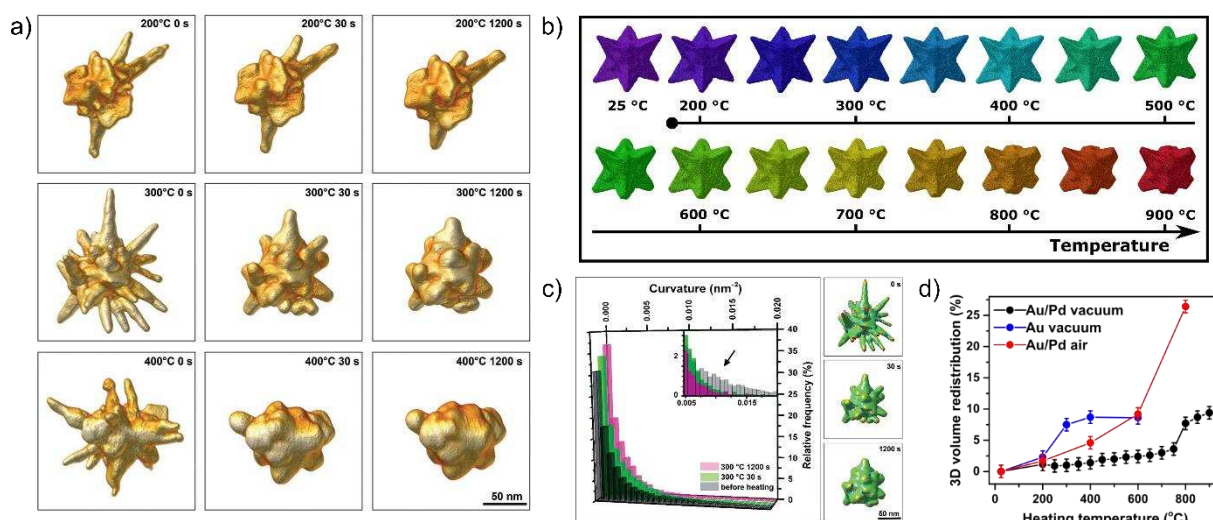


Figure 3. Surface diffusion of metal nanoparticles captured by electron tomography. a) 3D visualizations of a Au NS before and after heating at 200°C, 300°C and 400°C. b) 3D visualization of the same AuPd octopod before heating (25°C) and after heating for 5 min at intermediate temperatures between 200°C and 900°C. c) Histograms illustrating the measured curvature of the Au NS after different durations of heating at 300°C. In the inset, a magnified 2D view of the histograms is shown highlighting the loss of high curvature as a function of temperature (black arrow). On the right, the curvature of the Au NS is visualized before heating, after 30 s and 1200 s of heating at 300°C, where red and blue represent high positive and high negative curvatures, respectively. d) Quantified redistributed volume for the same AuPd octopod from b) in vacuum (black, corresponding to the visualizations shown in a)), in air (red) and a pure Au octopod in vacuum (blue). a), c) Adapted with permission from ref. 33. Copyright 2018 Royal Society of Chemistry. b), d) Adapted with permission from ref. 2. Copyright 2019 American Chemical Society.

The reshaping behavior is obvious for the Au NSs (**Figure 3a**) and we also observed a morphology transformation for AuPd octopods in 3D (**Figure 3b**). Although the exact reshaping mechanism has not been fully unravelled yet,^{39–41} previous work identified curvature of the NP as an important parameter.⁴⁰ By having the complete 3D information at every reshaping step, we could unambiguously demonstrate for the NSs and octopods that indeed

volume got redistributed from areas of higher curvature (tips/branches) to areas of lower curvature (sides) resulting in an overall decrease of the NPs' curvature (**Figure 3c**). By tracking the redistributed volume quantitatively, we could compare the degree of reshaping under different stimuli. We hereby observed that the AuPd octopods underwent a different transformation in air (**Figure 3d**, red curve) than in vacuum (**Figure 3d**, black curve). The lower stability in air can likely be attributed to burning of the surface ligands and different stability of surface facets in air and vacuum. More important than the surrounding environment was the presence of Pd in the octopods, responsible for a tremendous increase in stability compared to Au-only octopods (**Figure 3d**, blue curve). These observations show that the initial morphology is not the only factor in the reshaping behavior and that for industrial applications additional factors need to be taken into account.

Reshaping of NPs has an immediate effect on their optical properties. For the Au NSs we showed that the loss in sharp tips resulted in a significant decrease in the 3D average electromagnetic field enhancement in the visible and near-infrared range, which is a major concern for plasmonic applications. This was possible by using the measured 3D morphology of the NSs at different time intervals as an input for electromagnetic simulations.⁴² Alternative to simulating the optical properties, those can also be directly measured inside the TEM by electron energy loss spectroscopy (EELS). For the AuPd octopods, we performed *in situ* EELS measurements to monitor the plasmonic changes as a function of temperature. We measured that the distal plasmon mode of the octopods barely lost intensity for temperatures up to 600°C, as expected for the rather minor morphological changes (**Figure 3d**).² Moreover, as the octopod branches stayed sharp, the field enhancement was localized at the tips even at 600°C. Although the addition of Pd led to a broadening of the plasmon resonance compared to pure Au octopods, AuPd octopods are nonetheless promising NPs for plasmonic applications that require high temperatures.

Next to monitoring surface diffusion, *in situ* electron tomography is also suited to quantify internal NPs' elemental diffusion of e.g. alloying materials. We can hereby use the so-called *Z* contrast in HAADF-STEM imaging as elements with different atomic numbers scatter electrons to different angles resulting in different intensities. For core-shell geometries of materials with different *Z* contrast, each voxel intensity in the 3D reconstruction can consequently be attributed to an element (**Figure 4a**, first column). Moreover, when the imaging conditions are not changed, the evolving voxel intensities can be used to quantify elemental diffusion inside the NPs as shown for three different NPs in **Figure 4a**.³ In this specific work, we heated the initial core-shell NPs at 450°C to induce alloying. The NPs were protected by a mesoporous silica shell to prevent NP reshaping. We quantified the progress of alloying by evaluating the spread in the 3D voxel histograms (**Figure 4b**, blue points). Furthermore, by fitting the experimental results to the outcome of diffusion simulations based on a discretization of Fick's law over the experimental voxel grid, we could calculate diffusion constants on a single NP level (**Figure 4b**, yellow solid curves). Diffusion constants of $1 - 3 \times 10^{-19} \text{ m}^2/\text{s}$ were in good agreement with tabulated bulk values.³ For smaller NP sizes, diffusion is expected to be sped up due to the size confinement.⁴³ In a follow-up work, we currently investigate the dependence of the diffusion speed on the size, shape and local composition of a large variety of core-shell geometries. Such a single NP study becomes possible due to a significant improvement in signal-to-noise ratio compared to alternative TEM techniques such as EDX tomography, but is limited to elements with sufficiently high *Z* contrast differences.

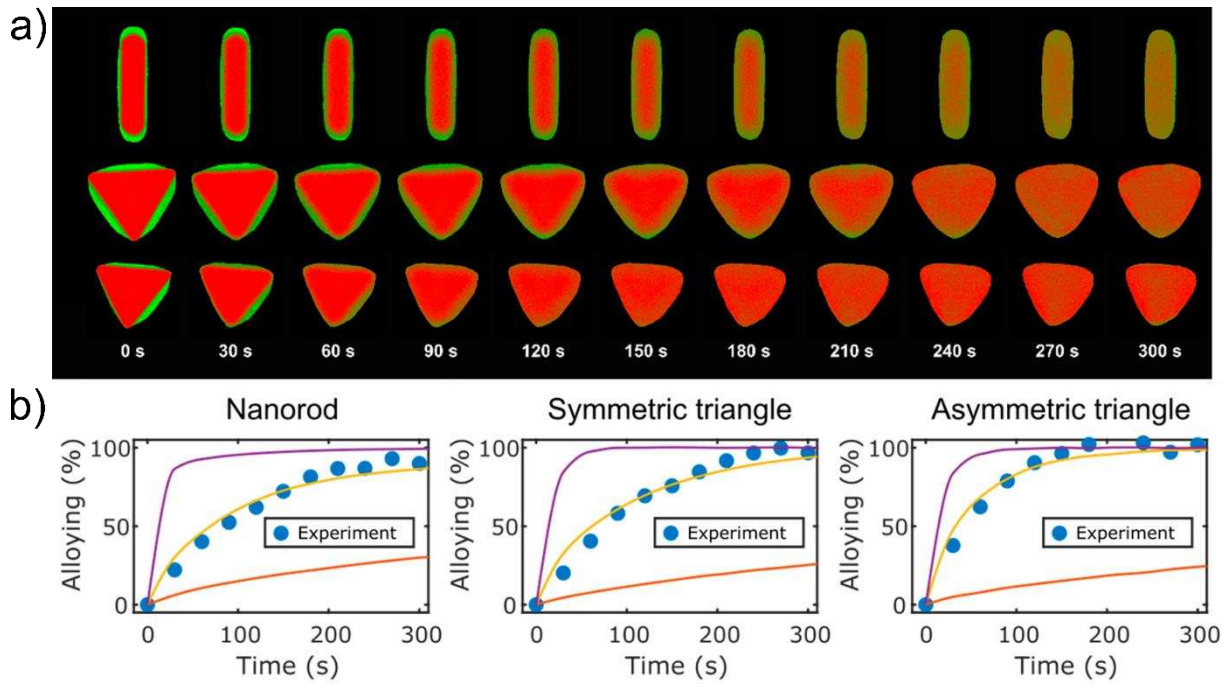


Figure 4. Internal elemental diffusion in $\text{SiO}_2\text{@Ag@Au}$ NPs of varying shapes measured by electron tomography (SiO_2 is not shown here). a) Slices through the 3D reconstructions of elemental distributions inside a nanorod, a symmetric, and an asymmetric nanotriangle, respectively, at different stages of alloying at 450°C . Pure green and red indicate Ag and Au, respectively. b) Quantified alloying progress based on the experimental data (blue points) and simulation results (solid lines). Diffusion coefficients of $1 \times 10^{-19} \text{ m}^2/\text{s}$ (nanorod), $1.5 \times 10^{-19} \text{ m}^2/\text{s}$ (symmetric triangle), and $3 \times 10^{-19} \text{ m}^2/\text{s}$ (asymmetric triangle) produced the best match with the experimental data (yellow curves). Purple and orange curves correspond to a diffusion coefficient of $1.0 \times 10^{-18} \text{ m}^2/\text{s}$ and $1.0 \times 10^{-20} \text{ m}^2/\text{s}$, respectively. Adapted with permission from ref. 3. Copyright 2019 American Chemical Society.

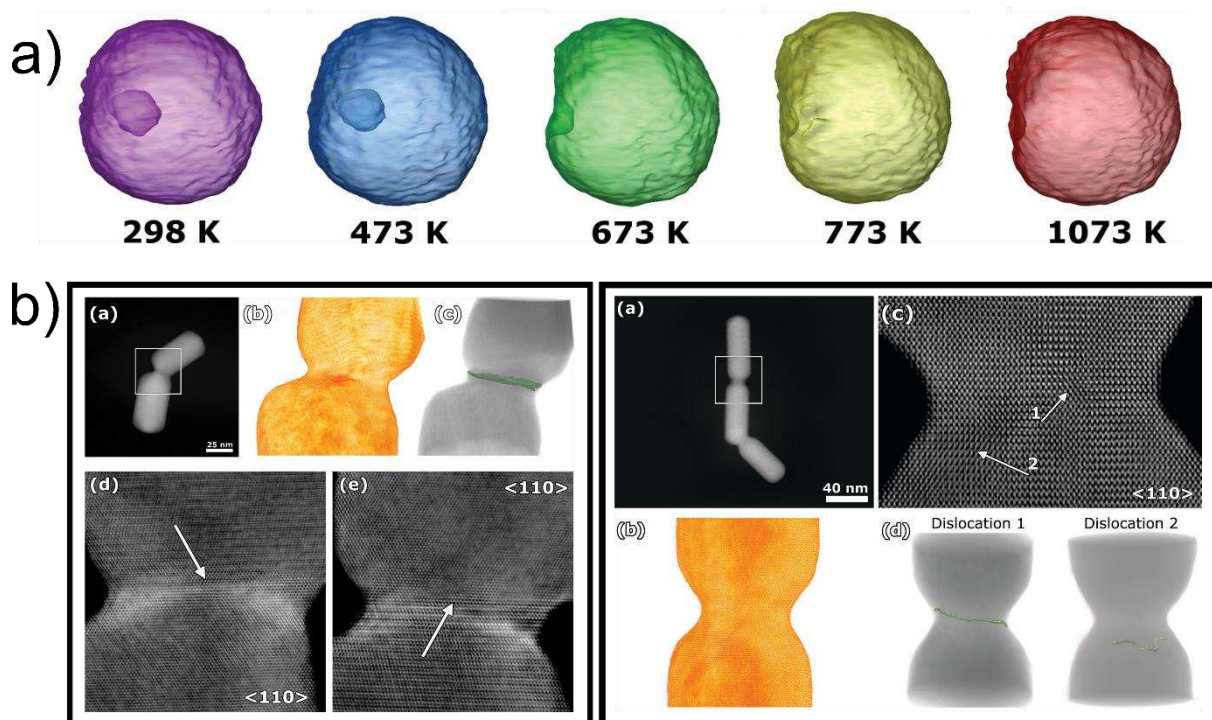


Figure 5. Laser-induced NP transformations captured by electron tomography. a) 3D visualizations of a Au NP with a cavity in the inside, introduced by nanosecond laser pulse excitation. The cavity migrated towards the closest surface during in situ heating inside the electron microscope at the indicated temperature for 5 min. b) Reconstructions with atomic resolution of gold nanorods welded together by femtosecond laser pulses. The left and right panel show welded nanorods with a grain boundary and dislocations at the interface, respectively. Adapted with permission from ref. 4 and 53. Copyright 2020 American Chemical Society.

Next to directly heating nanoparticles, intriguing transformations have been observed upon laser excitation of nanomaterials, not achievable by simply heating the material. Due to the ultrafast time scales of pulsed laser excitation, these transformations cannot be easily monitored *in situ*, but electron tomography is nonetheless indispensable to evaluate the laser-induced changes of NPs. It is worth mentioning that a few groups have built dedicated setups to excite the sample by ultrafast laser pulses inside the TEM.^{44–48} Here, we will focus on studies in which

the laser excitation has been performed outside the TEM. Among the variety of fascinating NP transformations that have been reported under pulsed laser excitation are reshaping, fragmentation, assembling, welding and even compositional changes.^{15,16,48-52} Recently, we observed that nanosecond pulsed irradiation under controlled conditions can introduce cavities inside Au NPs, which we confirmed by electron tomography (**Figure 5a**).⁵³ This phenomenon occurred for a specific interplay of excitation fluence and surfactant concentration. The nanocavity was stabilized by organic matter inside as directly proven by EELS measurements. Interestingly, the cavities migrated to the surface of the NP (**Figure 5a**) upon heating. MD simulations revealed that the presence of liquid material inside the cavity is responsible for such behavior, suggesting that the organic matter inside the cavity was a combination of solvent molecules and surfactants. Our results demonstrated that controlled nanosecond laser excitation can be used to trap matter from the surrounding medium, which can be subsequently released by heat or laser irradiation, indicating that these systems could potentially be used as drug delivery systems.

Femtosecond laser excitation can be employed to controllably weld assembled Au NRs together at the tips and hence creating novel structures, which could not be easily achieved by bottom-up synthesis.⁵⁴ Atomic resolution electron tomography gave detailed insight into the welding process (**Figure 5b**).⁴ The nanostructures exhibited a large range of welding angles and depending on the crystallographic orientation of the NRs, we observed defined defects at the interface between two welded NRs. Dislocations occurred for NRs with similar crystallographic orientations (**Figure 5b**, right panel) and grain boundaries otherwise (**Figure 5b**, left panel). The rest of the nanostructure remained defect-free. The welded NRs are also an excellent model system to measure the influence of a single defect on the plasmonic properties. Using single-particle low-loss EELS experiments on welded and single-crystalline Au NRs of similar plasmon resonance energies, we observed that a single crystal defect can cause a significant plasmon broadening (around 1.3 - 1.4 times at resonance energies around 1.2 - 1.3 eV). The

reduction of plasmonic strength due to a single crystal defect needs to be taken into account for plasmonic applications and for best performances single-crystalline NPs should be employed.

4. TRANSFORMATIONS CAPTURED BY ATOM COUNTING

One of the main challenges for electron tomography are experiments, where holders simply do not yield sufficient tilt ranges. This is the case for most in situ holders such as relatively bulky gas or liquid holders. For these cases, the method of atom counting combined with energy minimization, introduced in Section 2, creates new possibilities for the 3D characterization of materials. An example of the *in situ* approach based on atom counting is illustrated for imaging the transformation of a Au nanodumbbell into a nanorod when increasing the temperature to 330°C using an in situ heating holder.⁵⁵ The right tip of the nanodumbbell and nanorod before and after heating is shown in **Figures 6a,d**. These images were used for the atom counting/energy-minimization approach discussed in Section 2. The obtained 3D atomic models of the nanodumbbell and nanorod are shown along different directions in **Figures 6b,e** and **Figures 6c,f**, respectively. Orange and yellow arrows indicate the widths and heights of the surface facets, respectively. This extra information parallel to the incoming beam could only be obtained from the 3D atomic models and is hidden in the projection images. From **Figures 6b,e**, additional surface roughness is observed along the direction of the electron beam, resulting from the limited precision of the atom-counts, introduced by noise in the projection images. Nevertheless, surface facets could be clearly observed for the entire tip of the nanodumbbell and nanorod (**Figures 6c,f**). The results show that the nanoparticle was mainly composed of

{111}, {110}, and {100} facets, before as well as after heating. However, more low index facets were observed after heating.

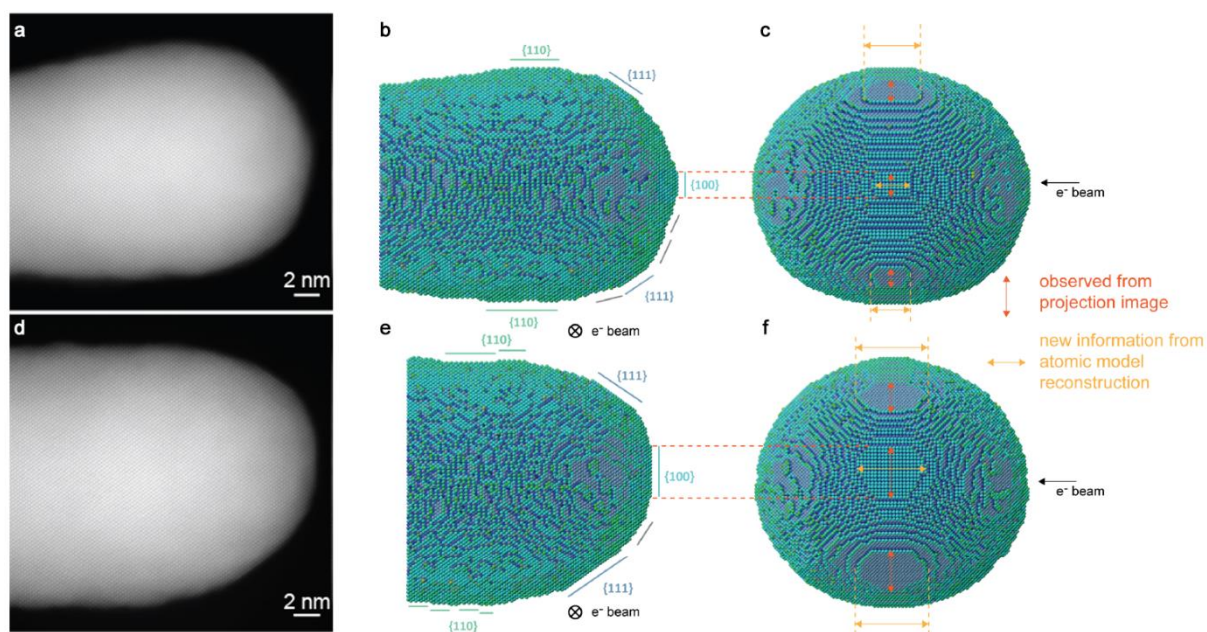


Figure 6. Atomic resolution ADF-STEM images and corresponding three-dimensional atomic models of a nanodumbbell/nanorod along different viewing directions (a,b,c) Au dumbbell before heating, (d,e,f) Au rod after heating to 330°C. The coloring of the Au atoms determines the nearest-neighbor coordination. Adapted with permission from ref. 55. Copyright 2017 Royal Society of Chemistry.

These results indicate the great potential of the technique for those studies where tilting of the holder to large angles is impossible. This is e.g. the case for the DENSsolutions Climate gas flow holder enabling pressures up to 1 bar and temperatures up to 1000°C. This holder clearly transforms the TEM into a true nanoreactor, but unfortunately the system cannot be used for conventional tilt tomography experiments. By applying atom counting combined with energy minimization, measuring variations of the 3D atomic structure of Pt nanoparticles under the flow of a selected gas became therefore possible. These particles are known to be a model catalyst for numerous gas phase reactions, which often occur in H₂ and O₂. Upon the adsorption of H₂ and O₂ molecules, surface energies are known to vary, which may lead to the

(de)stabilization of certain surface facets, consequently affecting the catalytic properties of the NPs.^{56,57} Morphological transformations of such particles during oxidation - reduction cycles have been previously investigated by *in situ* TEM, but these experiments only provided 2D projections of 3D objects.⁵⁷

Atom counting for HAADF-STEM images acquired in the gas environment is unfortunately far from straightforward. A key concern is the background related to the gas and the two SiN windows of the gas cell, lowering the quality of the HAADF-STEM images. Moreover, particle rotation while scanning causes image distortions, hampering a reliable quantification. To overcome these limitations, we acquired multiple consecutive images at high speed. However, as a consequence of the high acquisition speed, distortions are very strong. Therefore, we used deep convolutional neural networks (CNNs) to correct for these distortions.¹ Next, each series of individually corrected HAADF-STEM images was averaged after applying rigid and non-rigid alignment procedures. The resulting corrected and averaged images were of high enough quality to reliably count the number of atoms in each atomic column. Again, 3D starting configuration based on the counting results was generated by positioning the atoms in each atomic column symmetrically around a central plane. Finally, the 3D model was relaxed using MD simulations that employed the embedded atom method potential. **Figure 7** shows a Pt nanoparticle, in vacuum at 300°C (**Figure 7a**), in 1 bar of 5% H₂ in Ar flow (**Figure 7b**), and in a 1 bar O₂ environment (**Figure 7c**). To investigate the transformation during cycling, the switch from H₂ to O₂ was repeated several times using the same particle. The results for the second cycle are presented in **Figure 7d** (in a H₂ flow) and **Figure 7e** (in a O₂ flow). By determining the different types of facets within an error below 1.7%, we clearly identified morphology changes during that process. The amount of {110} facets was approximately 7% and did not change much with changing environment. Under H₂ flow, the presence of {100} and {111} facets increased, resulting in the more faceted appearance of the particle. In O₂, the more rounded morphology can be attributed to a decrease of the percentage of these facets and

a significant increase of higher order facets. Although the morphological changes were generally reversible upon repetitive cycling of H₂ and O₂, a small hysteresis effect was observed for the final change to O₂ (**Figure 7e**). Since the surface structure will influence the properties of the NPs, this quantitative methodology to measure 3D transformations of NPs in a relevant environment is highly relevant toward understanding e.g. catalytic activity, stability and selectivity.

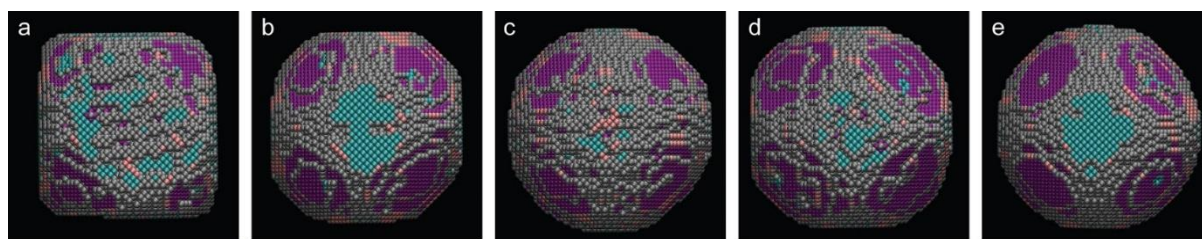


Figure 7. 3D structure of a Pt NP in vacuum (a) and in repeating different gaseous environments at 300°C, (b,d) in 5% H₂ in Ar; (c,e) in O₂. The atoms are colored, according to the type of facet: blue={100}, pink={110}, purple={111}, grey=higher index. Reprinted with permission from ref. 1. Copyright 2019 American Chemical Society.

5. CONCLUSIONS AND OUTLOOK

In this Account, we highlighted our recent progress on the observation of chemical and physical transformations of NPs in 3D inside the electron microscope. Developing robust methodologies for *in situ* studies is an important step towards routinely using them for more complex NPs. So far, we have fine-tuned methodologies on stable systems such as metal NPs. The next challenge will be to apply these methodologies to classes of materials for which degradation is very important, especially under the electron beam. Although specifically dominant for liquid cell TEM studies, we want to stress that the effect of the electron beam needs to be taken into account for all *in situ* studies.⁵⁸ For example, *in situ* heating experiments might be altered due to the transformation of surface ligands into an amorphous carbon layer and need to be compared to *ex situ* results.^{2,59} In fact, our 3D *in situ* methodologies can be beneficial to

understand electron beam damage and other degradation effects. Specifically, we believe that further 3D insight into the atomic restructuring of (in)organic metal halide perovskites under external stimuli will help to pinpoint the degradation mechanisms,³⁷ hence improving the stability of such systems. Moreover, investigations of organic material, such as the organic ligands at the surface of NPs, under external stimuli become feasible as well. These will give insight into the role of the chemical nature of the interface on the transformations of the inorganic nanocrystals.

Another important goal will be to make electron tomography suitable for observing dynamic processes in a more continuous manner than the current stop-and-go approach. To achieve this goal, NP transformations occurring during the acquisition time of a single tilt series can be incorporated in more advanced reconstruction algorithms, if they can be predicted to some extent. For very fast processes, e.g. pulsed laser excitation where the time resolution is too limited, tomography can be combined with MD simulation techniques to gain additional insight. For example, by acquiring a tilt series with atomic resolution before and after laser excitation on the same NP, structural changes can be visualized. When using the measured initial atomic distribution as an input for MD simulations, the missing dynamics can be retrieved.

The ultimate challenge for the field will be to track the movement of single atoms in 3D of application-relevant material systems under realistic conditions. On the one hand, the interaction of NPs with possible supports, as often used in catalysis, needs to be taken into account. On the other hand, the actual performance of the NP needs to be evaluated e.g. by measuring which species are formed during an *in situ* catalytic reaction when combined with a mass spectrometer. For these challenges, the 3D modelling based on 2D images will be crucial and needs to be evaluated for more anisotropic and supported NPs. Moreover, machine learning using a hidden Markov model will enable us to model structural changes over time and to fully exploit the temporal information available in the observations.⁶⁰ This unique approach will

result in a precise characterization of complex NPs in response to environmental stimuli. This is a prerequisite to understand the unique link between a material's structure and its properties, which is important for the design of a broad range of nanomaterials.

BIOGRAPHIES

Dr. Wiebke Albrecht received her PhD in Physics from Utrecht University in 2017 and works currently as a postdoctoral researcher at the University of Antwerp. Her research is focussed on heat and laser-induced transformations of anisotropic metal and semiconductor nanoparticles. Her current research interests are also directed at the correlation of optical and structural properties of nanoparticles.

Prof. dr. Sandra Van Aert received her Ph.D. at the Delft University of Technology (The Netherlands) in 2003 and is professor at the University of Antwerp since 2009. She initiated and expanded the use of statistical parameter estimation theory in the field of transmission electron microscopy. The goal is to quantitatively extract all information which is hidden in the experimental data. In this manner, unknown structure parameters can be estimated with high accuracy and precision. This enables one to measure 2D atomic column positions with subpicometer precision, to measure compositional changes at interfaces, to count atoms in an atomic column with single atom sensitivity, to unscramble mixtures of elements, and to reconstruct 3D structures with atomic resolution.

Prof. dr. Sara Bals received her PhD in Physics at the University of Antwerp in 2003 and is professor at the same university since 2007. Since 2015, she is the spokesperson of the electron microscopy group EMAT. She is an expert in the application and development of electron tomography for functional nanostructured materials. By combining state-of-the-art electron

microscopy with advanced 3D reconstruction algorithms, the positions and chemical nature of individual atoms in a broad variety of nanomaterials are routinely measured in her group. These measurements are now also performed under realistic conditions in heating, liquid or gas flow experiments to investigate nanomaterials under working conditions.

AUTHOR INFORMATION

Corresponding Author

* E-mail: sandra.vanaert@uantwerpen.be; sara.bals@uantwerpen.be

ACKNOWLEDGMENT

The authors acknowledge funding from the European Research Council under the European Union's Horizon 2020 research and innovation program (ERC Consolidator Grants #815128 – REALNANO and #770887 – PICOMETRICS), the Research Foundation Flanders (FWO, G.0267.18N) and the European Commission (EUSMI). The authors furthermore acknowledge funding from the European Union's Horizon 2020 research and innovation program, ESTEEM3. The authors also acknowledge contributions from all co-workers that have contributed over the years: Thomas Altantzis, Annick De Backer, Joost Batenburg and co-workers, Armand Béch , Eva Bladt, Lewys Jones and co-workers, Luis Liz-Marz n and co-workers, Ivan Lobato, Thais Milagres de Oliveira, Peter Nellist and co-workers, Hugo P rez Garza and co-workers, Alexander Skorikov, Sara Skrabalak and co-workers, Sandra Van Aert, Alfons van Blaaderen and co-workers, Hans Vanrompay, Staf Van Tendeloo and Johan Verbeeck.

REFERENCES

- (1) Altantzis, T.; Lobato, I.; De Backer, A.; B ch , A.; Zhang, Y.; Basak, S.; Porcu, M.; Xu, Q.; S nchez-Iglesias, A.; Liz-Marz n, L. M.; Van Tendeloo, G.; Van Aert, S.;

- Bals, S. Three-Dimensional Quantification of the Facet Evolution of Pt Nanoparticles in a Variable Gaseous Environment. *Nano Lett.* **2019**, *19*, 477–481.
<https://doi.org/10.1021/acs.nanolett.8b04303>.
- (2) Albrecht, W.; Bladt, E.; Vanrompay, H.; Smith, J. D.; Skrabalak, S. E.; Bals, S. Thermal Stability of Gold/Palladium Octopods Studied in Situ in 3D: Understanding Design Rules for Thermally Stable Metal Nanoparticles. *ACS Nano* **2019**, *13*, 6522–6530. <https://doi.org/10.1021/acsnano.9b00108>.
- (3) Skorikov, A.; Albrecht, W.; Bladt, E.; Xie, X.; van der Hoeven, J. E. S.; van Blaaderen, A.; Van Aert, S.; Bals, S. Quantitative 3D Characterization of Elemental Diffusion Dynamics in Individual Ag@Au Nanoparticles with Different Shapes. *ACS Nano* **2019**, *13*, 13421–13429. <https://doi.org/10.1021/acsnano.9b06848>.
- (4) Oliveira, T. M. De; Albrecht, W.; González-Rubio, G.; Altantzis, T.; Hoyos, I. P. L.; Béché, A.; Guerrero-Martínez, A.; Liz-Marzán, L. M.; Bals, S. 3D Characterization of Gold Nanorods after Welding under Femtosecond Laser Irradiation. *ACS Nano* **2020**, *14*, 12558–12570. <https://doi.org/10.1021/acsnano.0c02610>.
- (5) Heuer-Jungemann, A.; Feliu, N.; Bakaimi, I.; Hamaly, M.; Alkilany, A.; Chakraborty, I.; Masood, A.; Casula, M. F.; Kostopoulou, A.; Oh, E.; Susumu, K.; Stewart, M. H.; Medintz, I. L.; Stratakis, E.; Parak, W. J.; Kanaras, A. G. The Role of Ligands in the Chemical Synthesis and Applications of Inorganic Nanoparticles. *Chem. Rev.* **2019**, *119*, 4819–4880. <https://doi.org/10.1021/acs.chemrev.8b00733>.
- (6) Erni, R.; Rossell, M. D.; Kisielowski, C.; Dahmen, U. Atomic-Resolution Imaging with a Sub-50-pm Electron Probe. *Phys. Rev. Lett.* **2009**, *102*, 096101.
<https://doi.org/10.1103/PhysRevLett.102.096101>.
- (7) Batson, P. E.; Dellby, N.; Krivanek, O. L. Sub-Angstrom Resolution Using Aberration

- Corrected Electron Optics. *Nature* **2002**, *418*, 617–620.
- (8) Kabius, B.; Haider, M.; Uhlemann, S.; Schwan, E.; Urban, K.; Rose, H. First Application of a Spherical-Aberration Corrected Transmission Electron Microscope in Materials Science. *J. Electron Microsc. (Tokyo)*. **2002**, *51*, S51–S58.
<https://doi.org/10.1093/jmicro/51.supplement.s51>.
- (9) Haider, M.; Rose, H.; Uhlemann, S.; Schwan, E.; Kabius, B.; Urban, K. A Spherical-Aberration-Corrected 200 KV Transmission Electron Microscope. *Ultramicroscopy* **1998**, *75*, 53–60. [https://doi.org/10.1016/S0304-3991\(98\)00048-5](https://doi.org/10.1016/S0304-3991(98)00048-5).
- (10) Bals, S.; Goris, B.; Liz-Marzán, L. M.; Van Tendeloo, G. Three-Dimensional Characterization of Noble-Metal Nanoparticles and Their Assemblies by Electron Tomography. *Angew. Chemie - Int. Ed.* **2014**, *53*, 10600–10610.
<https://doi.org/10.1002/anie.201401059>.
- (11) Bals, S.; Goris, B.; De Backer, A.; Van Aert, S.; Van Tendeloo, G. Atomic Resolution Electron Tomography. *MRS Bull.* **2016**, *41*, 525–530.
<https://doi.org/10.1557/mrs.2016.138>.
- (12) Midgley, P. A.; Weyland, M. 3D Electron Microscopy in the Physical Sciences: The Development of Z-Contrast and EFTEM Tomography. *Ultramicroscopy* **2003**, *96*, 413–431. [https://doi.org/10.1016/S0304-3991\(03\)00105-0](https://doi.org/10.1016/S0304-3991(03)00105-0).
- (13) Midgley, P. A.; Dunin-Borkowski, R. E. Electron Tomography and Holography in Materials Science. *Nat. Mater.* **2009**, *8*, 271–280. <https://doi.org/10.1038/nmat2406>.
- (14) Zheng, H.; Meng, Y. S.; Zhu, Y. Frontiers of in Situ Electron Microscopy. *MRS Bull.* **2015**, *40*, 12–18. <https://doi.org/10.1557/mrs.2014.305>.
- (15) Albrecht, W.; Deng, T.-S.; Goris, B.; van Huis, M. A.; Bals, S.; van Blaaderen, A. Single Particle Deformation and Analysis of Silica-Coated Gold Nanorods before and

- after Femtosecond Laser Pulse Excitation. *Nano Lett.* **2016**, *16*, 1818–1825.
<https://doi.org/10.1021/acs.nanolett.5b04851>.
- (16) Albrecht, W.; Goris, B.; Bals, S.; Hutter, E. M.; Vanmaekelbergh, D.; van Huis, M. A.; van Blaaderen, A. Morphological and Chemical Transformations of Single Silica-Coated CdSe/CdS Nanorods upon Fs-Laser Excitation. *Nanoscale* **2017**, *9*, 4810–4818.
<https://doi.org/10.1039/C6NR09879G>.
- (17) Goris, B.; Roelandts, T.; Batenburg, K. J.; Heidari Mezerji, H.; Bals, S. Advanced Reconstruction Algorithms for Electron Tomography: From Comparison to Combination. *Ultramicroscopy* **2013**, *127*, 40–47.
<https://doi.org/10.1016/j.ultramic.2012.07.003>.
- (18) Bals, S.; Batenburg, K. J.; Liang, D.; Lebedev, O.; Van Tendeloo, G.; Aerts, A.; Martens, J. A.; Kirschhock, C. E. A. Quantitative Three-Dimensional Modeling of Zeolite through Discrete Electron Tomography. *J. Am. Chem. Soc.* **2009**, *131*, 4769–4773. <https://doi.org/10.1021/ja8089125>.
- (19) Möbus, G.; Doole, R. C.; Inkson, B. J. Spectroscopic Electron Tomography. *Ultramicroscopy* **2003**, *96*, 433–451. [https://doi.org/10.1016/S0304-3991\(03\)00106-2](https://doi.org/10.1016/S0304-3991(03)00106-2).
- (20) Zanaga, D.; Altantzis, T.; Polavarapu, L.; Liz-Marzán, L. M.; Freitag, B.; Bals, S. A New Method for Quantitative XEDS Tomography of Complex Heteronanostructures. *Part. Part. Syst. Charact.* **2016**, *33*, 396–403. <https://doi.org/10.1002/ppsc.201600021>.
- (21) Li, Z. Y.; Young, N. P.; Di Vece, M.; Palomba, S.; Palmer, R. E.; Bleloch, A. L.; Curley, B. C.; Johnston, R. L.; Jiang, J.; Yuan, J. Three-Dimensional Atomic-Scale Structure of Size-Selected Gold Nanoclusters. *Nature* **2008**, *451*, 46–48.
<https://doi.org/10.1038/nature06470>.
- (22) Van Aert, S.; Batenburg, K. J.; Rossell, M. D.; Erni, R.; Van Tendeloo, G. Three-

- Dimensional Atomic Imaging of Crystalline Nanoparticles. *Nature* **2011**, *470*, 374–377. <https://doi.org/10.1038/nature09741>.
- (23) Goris, B.; De Backer, A.; Van Aert, S.; Gómez-Graña, S.; Liz-Marzán, L. M.; Van Tendeloo, G.; Bals, S. Three-Dimensional Elemental Mapping at the Atomic Scale in Bimetallic Nanocrystals. *Nano Lett.* **2013**, *13*, 4236–4241. <https://doi.org/10.1021/nl401945b>.
- (24) Goris, B.; Bals, S.; Van den Broek, W.; Carbó-Argibay, E.; Gómez-Graña, S.; Liz-Marzán, L. M.; Van Tendeloo, G. Atomic-Scale Determination of Surface Facets in Gold Nanorods. *Nat. Mater.* **2012**, *11*, 930–935. <https://doi.org/10.1038/nmat3462>.
- (25) Sadan, M. B.; Houben, L.; Wolf, S. G.; Enyashin, A.; Seifert, G.; Tenne, R.; Urban, K. Toward Atomic-Scale Bright-Field Electron Tomography for the Study of Fullerene-like Nanostructures. *Nano Lett.* **2008**, *8*, 891–896. <https://doi.org/10.1021/nl073149i>.
- (26) Scott, M. C.; Chen, C. C.; Mecklenburg, M.; Zhu, C.; Xu, R.; Ercius, P.; Dahmen, U.; Regan, B. C.; Miao, J. Electron Tomography at 2.4-Ångström Resolution. *Nature* **2012**, *483*, 444–447. <https://doi.org/10.1038/nature10934>.
- (27) Chen, C. C.; Zhu, C.; White, E. R.; Chiu, C. Y.; Scott, M. C.; Regan, B. C.; Marks, L. D.; Huang, Y.; Miao, J. Three-Dimensional Imaging of Dislocations in a Nanoparticle at Atomic Resolution. *Nature* **2013**, *496*, 74–77. <https://doi.org/10.1038/nature12009>.
- (28) Goris, B.; De Beenhouwer, J.; De Backer, A.; Zanaga, D.; Batenburg, K. J.; Sánchez-Iglesias, A.; Liz-Marzán, L. M.; Van Aert, S.; Bals, S.; Sijbers, J.; Van Tendeloo, G. Measuring Lattice Strain in Three Dimensions through Electron Microscopy. *Nano Lett.* **2015**, *15*, 6996–7001. <https://doi.org/10.1021/acs.nanolett.5b03008>.
- (29) Yang, Y.; Chen, C. C.; Scott, M. C.; Ophus, C.; Xu, R.; Pryor Jr., A.; Wu, L.; Sun, F.; Theis, W.; Zhou, J.; Eisenbach, M.; Kent, P. R. C.; Sabirianov, R. F.; Zeng, H.; Ercius,

- P.; Miao, J. Deciphering Chemical Order/Disorder and Material Properties at the Single-Atom Level. *Nature* **2017**, *542*, 75–79. <https://doi.org/10.1038/nature21042>.
- (30) Willhammar, T.; Sentosun, K.; Mourdikoudis, S.; Goris, B.; Kurttepel, M.; Berex, M.; Lamoen, D.; Partoens, B.; Pastoriza-Santos, I.; Pérez-Juste, J.; Liz-Marzán, L. M.; Bals, S.; Van Tendeloo, G. Structure and Vacancy Distribution in Copper Telluride Nanoparticles Influence Plasmonic Activity in the Near-Infrared. *Nat. Commun.* **2017**, *8*, 14925. <https://doi.org/10.1038/ncomms14925>.
- (31) Migunov, V.; Ryll, H.; Zhuge, X.; Simson, M.; Strüder, L.; Batenburg, K. J.; Houben, L.; Dunin-Borkowski, R. E. Rapid Low Dose Electron Tomography Using a Direct Electron Detection Camera. *Sci. Rep.* **2015**, *5*, 14516. <https://doi.org/10.1038/srep14516>.
- (32) Roiban, L.; Li, S.; Aouine, M.; Tuel, A.; Farrusseng, D.; Epicier, T. Fast ‘Operando’ Electron Nanotomography. *J. Microsc.* **2018**, *269*, 117–126. <https://doi.org/10.1111/jmi.12557>.
- (33) Vanrompay, H.; Bladt, E.; Albrecht, W.; Béché, A.; Zakhozheva, M.; Sánchez-Iglesias, A.; Liz-Marzán, L. M.; Bals, S. 3D Characterization of Heat-Induced Morphological Changes of Au Nanostars by Fast in Situ Electron Tomography. *Nanoscale* **2018**, *10*, 22792–22801. <https://doi.org/10.1039/c8nr08376b>.
- (34) Albrecht, W.; Bals, S. Fast Electron Tomography for Nanomaterials. *J. Phys. Chem. C* **2020**, *124*, 27276–27286. <https://doi.org/10.1021/acs.jpcc.0c08939>.
- (35) Van Aert, S.; De Backer, A.; Martinez, G. T.; Goris, B.; Bals, S.; Van Tendeloo, G.; Rosenauer, A. Procedure to Count Atoms with Trustworthy Single-Atom Sensitivity. *Phys. Rev. B* **2013**, *87*, 064107. <https://doi.org/10.1103/PhysRevB.87.064107>.
- (36) De Backer, A.; van den Bos, K. H. W.; Van den Broek, W.; Sijbers, J.; Van Aert, S.

- StatSTEM: An Efficient Approach for Accurate and Precise Model-Based Quantification of Atomic Resolution Electron Microscopy Images. *Ultramicroscopy* **2016**, *171*, 104–116. <https://doi.org/10.1016/j.ultramic.2016.08.018>.
- (37) Bals, S.; Van Aert, S.; Romero, C. P.; Lauwaet, K.; Van Bael, M. J.; Schoeters, B.; Partoens, B.; Yücelen, E.; Lievens, P.; Van Tendeloo, G. Atomic Scale Dynamics of Ultrasmall Germanium Clusters. *Nat. Commun.* **2012**, *3*, 897. <https://doi.org/10.1038/ncomms1887>.
- (38) Petrova, H.; Perez Juste, J.; Pastoriza-Santos, I.; Hartland, G. V; Liz-Marzán, L. M.; Mulvaney, P. On the Temperature Stability of Gold Nanorods: Comparison between Thermal and Ultrafast Laser-Induced Heating. *Phys. Chem. Chem. Phys.* **2006**, *8*, 814–821. <https://doi.org/10.1039/b514644e>.
- (39) Cho, H.; Shin, J. W.; Ryoo, R. Atomic Scale Mechanisms Underlying Thermal Reshaping of Anisotropic Gold Nanocrystals Revealed by in Situ Electron Microscopy. *J. Phys. Chem. C* **2020**, *124*, 12855–12863. <https://doi.org/10.1021/acs.jpcc.0c04281>.
- (40) Taylor, A. B.; Siddiquee, A. M.; Chon, J. W. M. Below Melting Point Photothermal Reshaping of Single Gold Nanorods Driven by Surface Diffusion. *ACS Nano* **2014**, *8*, 12071–12079.
- (41) Link, S.; Wang, Z. L.; El-Sayed, M. A. How Does a Gold Nanorod Melt? *J. Phys. Chem. B* **2000**, *104*, 7867–7870. <https://doi.org/10.1021/jp0011701>.
- (42) Hohenester, U.; Trügler, A. MNPBEM – A Matlab Toolbox for the Simulation of Plasmonic Nanoparticles. *Comput. Phys. Commun.* **2012**, *183*, 370–381. <https://doi.org/10.1016/j.cpc.2011.09.009>.
- (43) Shibata, T.; Bunker, B. A.; Zhang, Z.; Meisel, D.; Vardeman II, C. F.; Gezelter, J. D. Size-Dependent Spontaneous Alloying of Au-Ag Nanoparticles. *J. Am. Chem. Soc.*

- 2002**, *124*, 11989–11996. <https://doi.org/10.1021/ja026764r>.
- (44) Pomarico, E.; Madan, I.; Berruto, G.; Vanacore, G. M.; Wang, K.; Kaminer, I.; García De Abajo, F. J.; Carbone, F. MeV Resolution in Laser-Assisted Energy-Filtered Transmission Electron Microscopy. *ACS Photonics* **2018**, *5*, 759–764. <https://doi.org/10.1021/acsp Photonics.7b01393>.
- (45) Wang, K.; Dahan, R.; Shentcis, M.; Kauffmann, Y.; Ben Hayun, A.; Reinhardt, O.; Tsesses, S.; Kaminer, I. Coherent Interaction between Free Electrons and a Photonic Cavity. *Nature* **2020**, *582*, 50–54. <https://doi.org/10.1038/s41586-020-2321-x>.
- (46) Hassan, M. T.; Baskin, J. S.; Liao, B.; Zewail, A. H. High-Temporal-Resolution Electron Microscopy for Imaging Ultrafast Electron Dynamics. *Nat. Photonics* **2017**, *11*, 425–430. <https://doi.org/10.1038/nphoton.2017.79>.
- (47) Rossouw, D.; Bugnet, M.; Botton, G. A. Structural and Electronic Distortions in Individual Carbon Nanotubes under Laser Irradiation in the Electron Microscope. *Phys. Rev. B* **2013**, *87*, 125403. <https://doi.org/10.1103/PhysRevB.87.125403>.
- (48) Voss, J. M.; Olshin, P. K.; Charbonnier, R.; Drabbels, M.; Lorenz, U. J. In Situ Observation of Coulomb Fission of Individual Plasmonic Nanoparticles. *ACS Nano* **2019**, *13*, 12445–12451. <https://doi.org/10.1021/acsnano.9b06664>.
- (49) González-Rubio, G.; Díaz-Núñez, P.; Rivera, A.; Prada, A.; Tardajos, G.; González-Izquierdo, J.; Bañares, L.; Llombart, P.; Macdowell, L. G.; Palafox, M. A.; Liz-Marzán, L. M.; Peña-Rodríguez, O.; Guerrero-Martínez, A. Femtosecond Laser Reshaping Yields Gold Nanorods with Ultranarrow Surface Plasmon Resonances. *Science* **2017**, *358*, 640–644. <https://doi.org/10.1126/science.aan8478>.
- (50) Zuev, D. A.; Makarov, S. V.; Mukhin, I. S.; Milichko, V. A.; Starikov, S. V.; Morozov, I. A.; Shishkin, I. I.; Krasnok, A. E.; Belov, P. A. Fabrication of Hybrid Nanostructures

- via Nanoscale Laser-Induced Reshaping for Advanced Light Manipulation. *Adv. Mater.* **2016**, *28*, 3087–3093. <https://doi.org/10.1002/adma.201505346>.
- (51) González-Rubio, G.; Guerrero-Martínez, A.; Liz-Marzán, L. M. Reshaping, Fragmentation, and Assembly of Gold Nanoparticles Assisted by Pulse Lasers. *Acc. Chem. Res.* **2016**, *49*, 678–686. <https://doi.org/10.1021/acs.accounts.6b00041>.
- (52) Link, S.; Burda, C.; Nikoobakht, B.; El-Sayed, M. A. Laser-Induced Shape Changes of Colloidal Gold Nanorods Using Femtosecond and Nanosecond Laser Pulses. *J. Phys. Chem. B* **2000**, *104*, 6152–6163. <https://doi.org/10.1021/jp000679t>.
- (53) González-Rubio, G.; Milagres De Oliveira, T.; Albrecht, W.; Díaz-Núñez, P.; Castro-Palacio, J. C.; Prada, A.; González, R. I.; Scarabelli, L.; Bañares, L.; Rivera, A.; Liz-Marzán, L. M.; Peña-Rodríguez, O.; Bals, S.; Guerrero-Martínez, A. Formation of Hollow Gold Nanocrystals by Nanosecond Laser Irradiation. *J. Phys. Chem. Lett.* **2020**, *11*, 670–677. <https://doi.org/10.1021/acs.jpcclett.9b03574>.
- (54) González-Rubio, G.; González-Izquierdo, J.; Bañares, L.; Tardajos, G.; Rivera, A.; Altantzis, T.; Bals, S.; Peña-Rodríguez, O.; Guerrero-Martínez, A.; Liz-Marzán, L. M. Femtosecond Laser-Controlled Tip-to-Tip Assembly and Welding of Gold Nanorods. *Nano Lett.* **2015**, *15*, 8282–8288. <https://doi.org/10.1021/acs.nanolett.5b03844>.
- (55) De Backer, A.; Jones, L.; Lobato, I.; Altantzis, T.; Goris, B.; Nellist, P. D.; Bals, S.; Van Aert, S. Three-Dimensional Atomic Models from a Single Projection Using Z-Contrast Imaging: Verification by Electron Tomography and Opportunities. *Nanoscale* **2017**, *9*, 8791–8798. <https://doi.org/10.1039/C7NR02656K>.
- (56) Shi, A. C.; Masel, R. I. The Effects of Gas Adsorption on Particle Shapes in Supported Platinum Catalysts. *J. Catal.* **1989**, *120*, 421–431. [https://doi.org/10.1016/0021-9517\(89\)90282-0](https://doi.org/10.1016/0021-9517(89)90282-0).

- (57) Cabié, M.; Giorgio, S.; Henry, C. R.; Axet, M. R.; Philippot, K.; Chaudret, B. Direct Observation of the Reversible Changes of the Morphology of Pt Nanoparticles under Gas Environment. *J. Phys. Chem. C* **2010**, *114*, 2160–2163.
<https://doi.org/10.1021/jp906721g>.
- (58) Egerton, R. F. Radiation Damage to Organic and Inorganic Specimens in the TEM. *Micron* **2019**, *119*, 72–87. <https://doi.org/10.1016/j.micron.2019.01.005>.
- (59) Albrecht, W.; van de Glind, A.; Yoshida, H.; Isozaki, Y.; Imhof, A.; van Blaaderen, A.; de Jongh, P. E.; de Jong, K. P.; Zečević, J.; Takeda, S. Impact of the Electron Beam on the Thermal Stability of Gold Nanorods Studied by Environmental Transmission Electron Microscopy. *Ultramicroscopy* **2018**, *193*, 97–103.
<https://doi.org/10.1016/j.ultramic.2018.05.006>.
- (60) De wael, A.; De Backer, A.; Jones, L.; Varambhia, A.; Nellist, P. D.; Aert, S. Van. Measuring Dynamic Structural Changes of Nanoparticles at the Atomic Scale Using Scanning Transmission Electron Microscopy. *Phys. Rev. Lett.* **2020**, *124*, 106105.
<https://doi.org/10.1103/PhysRevLett.124.106105>.

